

Multi-layer Unmanned Aerial Vehicle Networks: Modeling and Performance Analysis

Dongsun Kim, Jemin Lee, *Member, IEEE*, and Tony Q. S. Quek, *Fellow, IEEE*

Abstract—Since various types of unmanned aerial vehicles (UAVs) with different hardware capabilities are introduced, we establish a foundation for the multi-layer aerial network (MAN). First, the MAN is modeled as K layer ANs, and each layer has UAVs with different densities, floating altitudes, and transmission power. To make the framework applicable for various scenarios in MAN, we consider the transmitter- and the receiver-oriented node association rules as well as the air-to-ground and air-to-air channel models, which form line of sight links with a location-dependent probability. We then newly analyze the association probability, the main link distance distribution, successful transmission probability (STP), and area spectral efficiency (ASE) of MAN. The upper bounds of the optimal densities that maximize STP and ASE are also provided. Finally, in the numerical results, we show the optimal UAV densities of an AN that maximize the ASE and the STP decrease with the altitude of the network. We also show that when the total UAV density is fixed for two layer AN, the use of single layer in higher(lower) altitude only for all UAVs can achieve better performance for low(high) total density case, otherwise, distributing UAVs in two layers, i.e., MAN, achieves better performance.

Index Terms—Aerial networks, multiple network layer, unmanned aerial vehicles, stochastic geometry, line of sight (LoS) probability.

I. INTRODUCTION

Recent development of the unmanned aerial vehicle (UAV) technologies enables the UAV to play various roles in the wireless networks. The UAVs are expected to work as temporal base stations in case of the disaster and the data demanding events [2], and the data acquisition for the crowd surveillance can also be done by UAVs [3]. Furthermore, the UAVs can act as a relay for unreliable direct link case [4]. As such demands on the UAV communications and the number of UAVs increase, the research for the reliable aerial network (AN) must be preceded.

The UAV based wireless communication has been studied in [5]–[10] after modeling the wireless channel and the mobility, which are different from those of the terrestrial networks. In [5], the probability that a link forms line of sight (LoS), i.e., the LoS probability, is modeled, which is determined by the angle from the ground, and also proposed the optimal UAV deployment that maximizes the coverage

area. The pathloss and the channel gain of the link between a UAV and a ground node are studied in [6]. In [7], the LoS probability is provided for the link between UAVs, which have different altitudes. Considering LoS channel, device-to-device communications, secrecy capacity UAV-aided communication systems, and UAV to ground communication in presence of interferer are studied in [8], [9], and [10], respectively. However, the studies mentioned above have considered only the small number of UAVs, which show the performance of the limited UAV communication scenarios.

Recently, the researches on the ANs, which is the wireless networks consisting of multiple UAVs, have been presented in [11]–[22]. For those works, the stochastic geometry, which is a widely-used tool for randomly distributed nodes [23], has been used. The Poisson point process (PPP)-based ANs model is presented and studied in [11]–[13], and the LoS and non-line of sight (NLoS) channels are considered for the air-to-ground (A2G) communications in [11] and [12]. Furthermore, the research on the coexistence of ANs with the terrestrial network is presented in [16]–[22]. In these works, the terrestrial network is modeled by a PPP and the distribution of UAVs is modeled by 3-D PPP [16]–[18] and 2-D PPP [19], [20]. Especially, in [21] and [22], the random distribution of users are also considered and modeled by a clustering point process (for disaster area or temporal data demanding events like concert) [21] and a PPP [22]. However, most of these works did not consider the multiple layer structure of AN, of each layer has different types of UAVs.

The ANs can have various types of UAVs with different floating altitudes and transmission power depending on their hardware constraints [24], which leads to the *multiple layer structure* in AN. The multiple layer structure can also be useful and required for better resource management and reliable communications, especially when the number of UAVs and UAV-related applications increase. Recently, the multiple layer structure for UAV communications has been considered in [14], [15], and [22]. In [14] and [15], the UAVs are used as relays [14] or downlink base stations to improve the downlink spectral efficiency [15]. However, a analysis result on the performance has not been provided, especially in terms of the successful transmission probability (STP) or the area spectral efficiency (ASE) of the multiple layer structure AN. In [22], the spectral efficiency of multiple layer structure AN was analyzed, by focusing on the communications of ground base stations, which are assisted by UAVs. However, in [22], only the performance of the single layer AN case is provided in the simulation results and the communication between UAVs are not considered, which fails to fully explore the efficient

D. Kim and J. Lee are with the Department of Information and Communication Engineering, Daegu Gyeongbuk Institute of Science and Technology, Daegu 42988, South Korea (e-mail: yidaever@dgist.ac.kr; jmn-lee@dgist.ac.kr).

T. Q. S. Quek is with Information Systems Technology and Design Pillar, Singapore University of Technology and Design, Singapore 487372 (e-mail: tonyquek@sutd.edu.sg).

Part of this paper was presented at the IEEE Global Communications Conference, UAE, December 2018 [1].

design of the multiple layer AN.

Therefore, in this paper, we consider the multi-layer aerial network (MAN), and provide a framework for the efficient design of the MAN. We first model the MAN, which is composed of K layers of ANs including UAVs with different transmission power, spatial densities, and floating altitudes. We then analyze the STP and the ASE of the MAN, and explore how to design the MAN to maximize its performance. The contribution of this work can be summarized as follows.

- Differently to prior works on aerial networks and terrestrial heterogeneous networks, we model the MAN by considering both the node association rules and channel model, suitable for various scenarios of the MAN. Specifically, according to the association subject, we consider two types: the *transmitter-oriented* association (e.g., when a transmitting UAV selects the best receiving base station (BS)) and the *receiver-oriented* association (e.g., when a receiving UAV selects the best transmitting BS). Furthermore, we consider both air-to-air (A2A) and A2G channels, which form LoS links with a certain probability, determined by not only the link distance but also the UAV altitude.
- We newly analyze the Laplace transform of the interference considering LoS and NLoS channels with the LoS probability, and provide that of the interference from same layer UAVs in a closed form. Note that the multiple layer structure has been considered for terrestrial networks, called as the heterogeneous networks [25]–[27], and the Laplace transform of the interference has also been analyzed. However, as the node association rules and the channel model, suitable for MAN, are used in this work, the analysis has been newly performed.
- We then analyze the STP and the ASE of the MAN using stochastic geometry. We also provide the upper bound of the optimal transmitting UAV densities for each layers, which maximize the STP and the ASE. This is the first work, optimizing the node density of AN, to the best knowledge of the authors.
- We finally provide insights on the efficient design of MAN via numerical results. Specifically, we provide the optimal altitude and the densities of UAV in each layer in terms of the STP and the ASE, and also show when the multiple layer structure of AN can achieve better performance than the single layer AN.

II. SYSTEM MODEL

In this section, we present the system model of a MAN including the network description and the channel model. Furthermore, we describe the node association rules and present the probability distribution function (PDF) of the main link distance.

A. Multi-layer Aerial Network Structure

We consider a MAN, which consists of K layers of AN at different altitudes as shown in Fig. 1. We denote \mathcal{K} as the set of layers constituting the MAN, i.e., $\mathcal{K} = \{0, 1, \dots, K\}$, where layer 0 is the terrestrial network. We assume UAVs

TABLE I
NOTATIONS USED THROUGHOUT THE PAPER.

Notation	Definition
\mathcal{K}	Set of layers constituting the MAN
h_k	altitude of the k -layer nodes
P_k	Transmission power of the k -layer nodes
$\lambda_{k,\text{Rx(Tx)}}$	Density of the receiver(transmitter) in the k -layer
$\Phi_{k,\text{Rx(Tx)}}$	Distribution of the receiver(transmitter) in the k -layer
$c \in \{\text{L}, \text{N}\}$	Indicator whether the channel is LoS or NLoS
$\alpha^{(c)}$	Pathloss exponent of channel c
$G^{m(c)}$	Channel gain of channel c
$\rho_{ij}^{(c)}(x)$	Probability that link between the i -layer receiver and the j -layer transmitter is under channel environment c when the link distance is x
$\tau = oa$	Communication node association rule defined by o and a
$o \in \{\text{r}, \text{t}\}$	Node association rule that indicates whether the communication is the receiver-oriented or the transmission oriented association
$a \in \{\text{n}, \text{s}\}$	Node association rule that indicates whether the node with the the nearest distance or the strongest power is selected
$\mathcal{A}_{ij,\tau}^{(c)}$	Probability that the main link is established between the i and j -layer nodes under channel c using association rule τ
$Y_{ij,\tau}^{(c)}$	Random variable that represents the main link distance given association $\mathcal{A}_{ij,\tau}^{(c)}$
$I_{ij}^{(c)}$	Interference to the i -layer receiver from j -layer transmitters in the channel c
\mathcal{I}_i	Sum of the interference and noise to the i -layer receiver
χ	Distance that indicates the area where the interferer cannot exist
$\varepsilon_{ij,\tau}^{(c)}(y)$	Event when the main link is established between i and j -layer with distance y using the node association rule τ
$\mathcal{L}_{I \varepsilon_{ij,\tau}^{(c)}}(y)$	Laplace transform of the I in the event of $\varepsilon_{ij,\tau}^{(c)}(y)$
$p_{ij,\tau}^{(c)}(y)$	STP in the event of $\varepsilon_{ij,\tau}^{(c)}(y)$
$\mathcal{P}_{k,\tau}$	STP of the k -layer in the MAN
$\mathcal{S}_{k,\tau}$	STP of the k -layer in the MAN [bps/Hz/m ²]
$\lambda_{j,\text{Tx}}^{b,\mathcal{P}_{k,\tau}(\mathcal{S}_{k,\tau})}$	Upper bound of the optimal transmitter density in the j -layer that maximizes the STP(ASE) of k -layer

in ANs are distributed according to PPPs such as in [19], [28] as well as the ground nodes in the terrestrial network [23]. Specifically, in the k -layer, the node locations follow a homogeneous PPP Φ_k with density λ_k , and they are at the fixed altitude h_k and transmit with the power P_k . In the k -layer, nodes act as either a receiver or a transmitter, where the set of the receivers and the transmitters are denoted by $\Phi_{k,\text{Rx}}$ and $\Phi_{k,\text{Tx}}$. Similarly, the densities of the receivers and the transmitters in the k -layer are given by $\lambda_{k,\text{Rx}}$ and $\lambda_{k,\text{Tx}}$. Here, $\Phi_k = \Phi_{k,\text{Rx}} + \Phi_{k,\text{Tx}}$ and $\lambda_k = \lambda_{k,\text{Rx}} + \lambda_{k,\text{Tx}}$. The altitude of

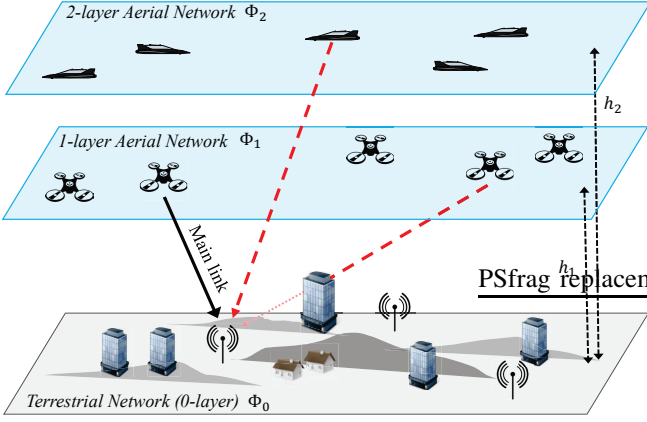


Fig. 1. An example of two layer MAN with ground receivers (i.e., 0-layer). The black lines represent the main link and red dashed lines represent interference links.

nodes in the 0-layer (i.e., the terrestrial layer) is $h_0 = 0$ and altitudes of other layers are $h_k \geq 0$ for $k \in \mathcal{K}$. In addition, the altitude between the i -layer and the j -layer is denoted by $h_{ij} = |h_i - h_j|$.

B. Channel Model

In the terrestrial network, where the transmitter and the receiver are on the ground, the channel is generally modeled as NLoS links. However, in the MAN, we have the communication between a UAV and a ground node and the communication between UAVs. For those communications, we consider both LoS and NLoS links, which are affected by the existence of obstacles (e.g., buildings) between the transmitter and the receiver [5], [7] by following the ITU model [29]. In this paper, we define the probability of forming LoS channel as the LoS probability $\rho_{ij}^{(L)}(x)$ and the probability of forming NLoS channel as the NLoS probability $\rho_{ij}^{(N)}(x) = 1 - \rho_{ij}^{(L)}(x)$, where a receiver and a transmitter are in the i -layer and the j -layer, respectively, and the link distance is x . From [5], the LoS probability is given by

$$\rho_{ij}^{(L)}(x) = \prod_{n=0}^m \left[1 - \exp \left(- \frac{[\max(h_i, h_j) - \frac{(n+1/2)h_{ij}}{m+1}]^2}{2\xi^2} \right) \right] \quad (1)$$

where $m = \text{floor} \left(\sqrt{(x^2 - h_{ij}^2)\mu\nu} - 1 \right)$. Here, μ , ν , and ξ are the parameters related to the environments [29]. Specifically, μ is the ratio of area covered by buildings to total area, ν is the mean number of buildings per unit area, and ξ is the average altitude of the buildings. The LoS probability can also be approximately determined using the sigmoid function based approximation [5], [30].¹ Specifically, for the A2G channel

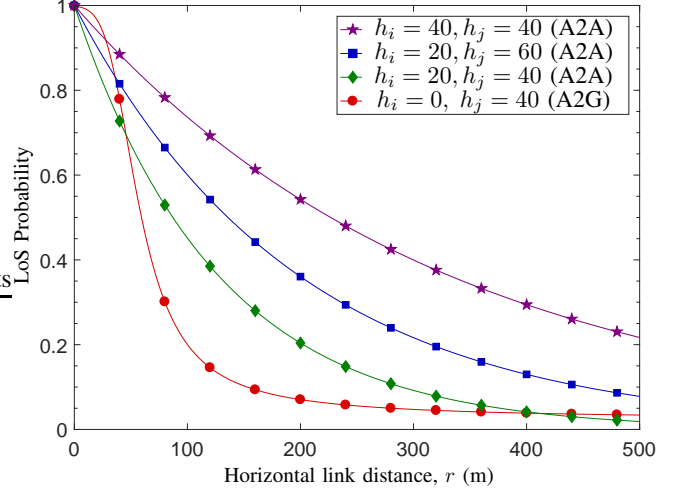


Fig. 2. LoS channel probability according to the horizontal distance r with different receiver and transmitter altitudes h_i and h_j .

(i.e., i or $j=0$, $i \neq j$), $\rho_{ij}^{(L)}(x)$ is given by [5]

$$\rho_{ij}^{(L)}(x) \approx \frac{1}{1 + \iota \exp \left[-\kappa \left[\sin^{-1} \left(\frac{h_{ij}}{x} \right) - \iota \right] \right]} \quad (2)$$

where ι and κ are related to ν , μ , and ξ [5]. For the A2A channel (i.e., i and $j \neq 0$), using the exponential function based approximation $\rho_{ij}^{(L)}(x)$ is given by [30]

$$\rho_{ij}^{(L)}(x) \approx \begin{cases} \left(1 - \exp \left\{ -\frac{h_{ij}^2}{2\xi^2} \right\} \right)^{x\sqrt{\nu\mu}} & \text{for } i = j, \\ \left(1 - \frac{\sqrt{2\pi\xi}}{h_{ij}} \left| Q \left(\frac{h_i}{\xi} \right) - Q \left(\frac{h_j}{\xi} \right) \right| \right)^{\sqrt{(x^2 - h_{ij}^2)\nu\mu}} & \text{for } i \neq j, \end{cases} \quad (3)$$

where $Q(x) = \int_x^\infty \frac{1}{\sqrt{2\pi}} \exp \left(-\frac{x^2}{2} \right) dx$. Especially, the LoS channel between ground nodes is given by $\rho_{ij}^{(L)}(x) = 0$.

From (2) and (3), we can see that the LoS probability is affected by both the horizontal distance and the altitude difference between the transmitter and the receiver, and this is also shown in Fig. 2. Figure 2 show the LoS probability as a function of the horizontal distance $r = \sqrt{x^2 - h_{ij}^2}$ for A2A and A2G channels in the dense urban environment.² We observe that the LoS probability decreases with r since the larger distance generally has more blockages, which causes the NLoS environment. On the contrary, the LoS probability increases not only with the altitude difference between the transmitter and receiver, h_{ij} , but also with altitudes of the transmitter and the receiver, h_i and h_j .

Based on the LoS probability, we define $\Phi_{ij,\text{Tx}}^{(L)}$ and $\Phi_{ij,\text{Tx}}^{(N)}$ as the set of transmitters in the j -layer which have LoS and NLoS channels to a receiver in the i -layer. Similarly, we define $\Phi_{ij,\text{Rx}}^{(L)}$ and $\Phi_{ij,\text{Rx}}^{(N)}$ as the set of receivers in the i -layer, which have LoS and NLoS channels to a transmitter in the j -layer, respectively. Here, the density of $\Phi_{ij,\text{Tx}}^{(c)}$ and $\Phi_{ij,\text{Rx}}^{(c)}$ for given link distance x becomes $2\pi x \lambda_{j,\text{Tx}} \rho_{ij}^{(c)}(x)$ and

¹Similar result with the same approach is provided in the [7], however, we follow the [30] to provide well-matched approximation with our model.

²The parameters used in this figure are $\mu = 0.5$, $\nu = 3 \times 10^{-4}$ (buildings/m²), $\xi = 20$ (m), $a = 12.0810$, and $b = 0.1139$ [5].

$2\pi x \lambda_{i,\text{Rx}} \rho_{ij}^{(c)}(x)$, $\forall c = \{L, N\}$, respectively.

The pathloss exponents for LoS and the NLoS channels are denoted by $\alpha^{(L)}$ and $\alpha^{(N)}$, respectively, and generally, $2 \leq \alpha^{(L)} \leq \alpha^{(N)}$. We also consider the Nakagami- m fading for LoS and the NLoS channels, of which channel gains are respectively presented by $G^{(L)} \sim \Gamma(m^{(L)}, \frac{1}{m^{(L)}})$ and $G^{(N)} \sim \Gamma(m^{(N)}, \frac{1}{m^{(N)}})$. Here, we use $m^{(N)} = 1$, which gives Rayleigh fading, i.e., $G^{(N)} \sim \exp(1)$, while $m^{(L)} \geq 1$.

C. Communication Node Association Rules

For node association rules, we consider two components o and a :

- 1) association subject o (whether a transmitter/receiver selects a receiver/transmitter); and
- 2) association criterion a (whether the node with strongest power or the nearest distance is selected).

In a MAN, a UAV may need to receive data from a ground base station and a UAV. For those cases, the UAV (i.e., receiver) can select the best transmitter for reliable communication and we call it as the *receiver-oriented* association, denoted by $o = r$. On the other hand, a UAV may need to transmit to a ground base station or a UAV. For those cases, the UAV (i.e., transmitter) can select the best receiver, and we call it as the *transmitter-oriented* association, denoted by $o = t$. For the selection criterion a , we consider both the nearest distance association and the strongest power association, denoted by $a = n$ and $a = s$, respectively. Note that the nearest and the strongest power associations have been generally used in wireless networks [31].

Based on the node association rule $\tau = oa$, the coordinate of the associated node for a node at \mathbf{x} is defined as

$$\mathbf{x}_\tau = \begin{cases} \arg \max_{\mathbf{x} \in \Phi_{k,o}, k \in \mathcal{K}} B_k |\mathbf{x} - \hat{\mathbf{x}}|^{-1} & \text{for } a = n, \\ \arg \max_{\mathbf{x} \in \Phi_{k,o}, k \in \mathcal{K}} B_k |\mathbf{x} - \hat{\mathbf{x}}|^{-\alpha_{\mathbf{x}}} & \text{for } a = s, \end{cases} \quad (4)$$

where B_k is the association bias of k -layer, $\alpha_{\mathbf{x}}$ is the pathloss exponent of the link between a transmitter and a receiver where the node \mathbf{x} is involved. In (4), $\Phi_{k,o}$ is defined as $\Phi_{k,r} = \Phi_{k,\text{Tx}}$ and $\Phi_{k,t} = \Phi_{k,\text{Rx}}$.

D. Main Link Distance Distribution Analysis

In the conventional terrestrial networks, the PDF of the main link distance is determined by the transmission power, the pathloss exponent, and the link distance. However, in the AN, we need to consider the LoS/NLoS probabilities for the links. Using the association $\tau = oa$, the PDF of the main link distance is presented in the following lemma. We use $f_X(x)$, $F_X(x)$, and $\bar{F}_X(x)$ to represent the PDF, cumulative distribution function (CDF), and complementary cumulative distribution function (CCDF) of a random variable X , respectively.

Lemma 1: Using the node association rule τ , when main link is established between a receiver in the i -layer and a

transmitter in the j -layer under the channel environment c , the PDF of main link distance $Y_{ij,\tau}^{(c)}$ is given by

$$f_{Y_{ij,\tau}^{(c)}}(y) = \frac{f_{V_{ij,o}^{(c)}}(y)}{\mathcal{A}_{ij,\tau}^{(c)}} \prod_{\substack{k \in \mathcal{K}, c_o \in \{L,N\}, \\ (k,c_o) \neq (j,c)}} \bar{F}_{V_{ik,o}^{(c_o)}}(R_{j,k,a}^{(c,c_o)}(y)), \quad (5)$$

where $\mathcal{A}_{ij,\tau}^{(c)}$ is the association probability given by

$$\mathcal{A}_{ij,\tau}^{(c)} = \int_{x>0} f_{V_{ij,o}^{(c)}}(x) \prod_{\substack{k \in \mathcal{K}, c_o \in \{L,N\}, \\ (k,c_o) \neq (j,c)}} \bar{F}_{V_{ik,o}^{(c_o)}}(R_{j,k,a}^{(c,c_o)}(x)) dx. \quad (6)$$

Here, $V_{ik,o}^{(c_o)}$ is the distance to the nearest node among the nodes in the k -layer AN under the channel environment $c_o \in \{L,N\}$ from a node in the i -layer, of which the CCDF and the PDF are given by

$$f_{V_{ik,o}^{(c_o)}}(v) = 2\pi \lambda_{k,o} v \rho_{ik}^{(c_o)}(v) \exp \left\{ - \int_{h_{ik}}^v 2\pi \lambda_{k,o} x \rho_{ik}^{(c_o)}(x) dx \right\},$$

$$\bar{F}_{V_{ik,o}^{(c_o)}}(v) = \exp \left[- \int_{h_{ik}}^{\max(v, h_{ik})} 2\pi \lambda_{k,o} x \rho_{ik}^{(c_o)}(x) dx \right], \quad (7)$$

where $f_{V_{ik,o}^{(c_o)}}(v) = 0$ if $v \geq h_{ik}$. In addition, $R_{j,k,a}^{(c,c_o)}(y)$ is given by

$$R_{j,k,a}^{(c,c_o)}(y) = \begin{cases} y B_k / B_j & \text{for } a = n, \\ (y^{\alpha^{(c)}} B_k / B_j)^{1/\alpha^{(c_o)}} & \text{for } a = s. \end{cases} \quad (8)$$

Proof: From the LoS probability, the density in the k -layer AN under the channel environment c_o in distance x is given by $2\pi x \lambda_{k,o} \rho_{ik}^{(c_o)}(x)$. Therefore, the CDF of $V_{ik,o}^{(c_o)}$ is given by

$$F_{V_{ik,o}^{(c_o)}}(v) \stackrel{(a)}{=} 1 - \exp \left\{ - \int_{h_{ik}}^{\max(v, h_{ik})} 2\pi x \lambda_{k,o} \rho_{ik}^{(c_o)}(x) dx \right\} \quad (9)$$

where (a) is from the void probability of PPP. From (9), we have (7).

In the nearest distance association case, the main link has the smallest distance, hence, the probability that main link is established as $\mathbf{x}_\tau \in \Phi_{ij,o}^{(c)}$ and the main link distance is smaller than y is given by

$$\begin{aligned} & \mathbb{P} \left(V_{ij,o}^{(c)} \leq y, \mathbf{x}_\tau \in \Phi_{ij,o}^{(c)} \mid a = n \right) \quad (10) \\ &= \int_0^y f_{V_{ij,o}^{(c)}}(v) \mathbb{P} \left(\mathbf{x}_\tau \in \Phi_{ij,o}^{(c)} \mid V_{ij,o}^{(c)} = v, a = n \right) dv \\ &\stackrel{(a)}{=} \int_0^y f_{V_{ij,o}^{(c)}}(v) \prod_{\substack{k \in \mathcal{K}, c_o \in \{L,N\}, \\ (k,c_o) \neq (j,c)}} \mathbb{P} \left[\frac{B_j}{v} \geq \frac{B_k}{V_{ik,o}^{(c_o)}} \right] dv \\ &= \int_0^y f_{V_{ij,o}^{(c)}}(v) \prod_{\substack{k \in \mathcal{K}, c_o \in \{L,N\}, \\ (k,c_o) \neq (j,c)}} \mathbb{P} \left[R_{j,k,n}^{(c,c_o)}(y) \leq V_{ik,o}^{(c_o)} \right] dv, \end{aligned}$$

where (a) is from (4). Here, for $y \rightarrow \infty$, the probability becomes equivalent to $\mathbb{P} \left[\mathbf{x}_\tau \in \Phi_{ij,o}^{(c)} \mid a = n \right]$, which gives association probability in (6). In the strongest power association case, the main link has the strongest signal power, hence, the

$$\mathcal{L}_{I_{ik}^{(c_0)}|\varepsilon_{ij,\tau}^{(c)}(y)}(s) = \exp \left[-2\pi\lambda_{k,\text{Tx}} \left\{ \int_{\max(\chi_{j,k,\tau}^{(c,c_0)}(y), h_{ik})}^{\infty} x \rho_{ik}^{(c_0)}(x) \left(1 - \left(\frac{1}{1 + \frac{sP_k x^{-\alpha^{(c_0)}}}{m^{(c_0)}}}} \right)^{m^{(c_0)}} \right) dx \right\} \right] \quad (14)$$

probability that main link is established as $\mathbf{x}_\tau \in \Phi_{ij,o}^{(c)}$ and the main link distance is smaller than y is given by

$$\begin{aligned} & \mathbb{P} \left(Y_{ij,\tau}^{(c)} \leq y, \mathbf{x}_\tau \in \Phi_{ij,o}^{(c)} \mid a = s \right) \quad (11) \\ & \stackrel{(a)}{=} \int_0^y f_{V_{ij,o}^{(c)}}(v) \prod_{\substack{k \in \mathcal{K}, c_0 \in \{\text{L}, \text{N}\}, \\ (k, c_0) \neq (j, c)}} \mathbb{P} \left[\frac{B_j}{v^{\alpha^{(c)}}} \geq \frac{B_k}{(V_{ik,o}^{(c_0)})^{\alpha^{(c_0)}}} \right] dv \\ & = \int_0^y f_{V_{ij,o}^{(c)}}(v) \prod_{\substack{k \in \mathcal{K}, c_0 \in \{\text{L}, \text{N}\}, \\ (k, c_0) \neq (j, c)}} \mathbb{P} \left[R_{j,k,s}^{(c,c_0)}(y) \leq V_{ik,o}^{(c_0)} \right] dv, \end{aligned}$$

where (a) is from (4). Therefore, we derived the association probability (6) by $y \rightarrow \infty$.

Finally, the CDF of main link distance $Y_{ij,\tau}^{(c)}$ is given by

$$F_{Y_{ij,\tau}^{(c)}}(y) = \mathbb{P} \left(V_{ij,o}^{(c)} \leq y, \mathbf{x}_\tau \in \Phi_{ij,o}^{(c)} \right) / \mathcal{A}_{ij,\tau}^{(c)}, \quad (12)$$

which gives (5). ■

III. INTERFERENCE ANALYSIS OF MANS

In this section, we analyze the Laplace transform of the interference in the MAN. In the MAN, the interference to the i -layer receiver from the transmitters in the k -layer AN, which have LoS links ($c_0 = \text{L}$) and NLoS links ($c_0 = \text{N}$) to the receiver is given by

$$I_{ik}^{(c_0)} = \sum_{\mathbf{x} \in \Phi_{ik,\text{Tx}}^{(c_0)}/\mathbf{x}_\tau} P_k G^{(c_0)} x^{-\alpha^{(c_0)}}, \quad \forall c_0 \in \{\text{L}, \text{N}\} \quad (13)$$

where x is the link distance. Let us define $\varepsilon_{ij,\tau}^{(c)}(y)$ as the event that using the rule τ , a i -layer receiver associates to a j -layer transmitter, and their link distance is y and channel environment is $c \in \{\text{L}, \text{N}\}$. From the definition of the interference and the node association rules, the Laplace transform of the interference is given for the case of $\varepsilon_{ij,\tau}^{(c)}(y)$ in the following lemma.

Lemma 2: In the case of $\varepsilon_{ij,\tau}^{(c)}(y)$, the the Laplace transform of the interference from transmitters in the k -layer AN under the channel environment c_0 is given by (14), which is presented on the top of this page, where $\chi_{j,k,\tau}^{(c,c_0)}(y)$ is given by

$$\chi_{j,k,\tau}^{(c,c_0)}(y) = \begin{cases} R_{j,k,a}^{(c,c_0)}(y) & \text{for } o = r, \\ 0 & \text{for } o = t, \end{cases} \quad (15)$$

where $R_{j,k,a}^{(c,c_0)}(y)$ is defined in (8).

Proof: In the case of $\varepsilon_{ij,\tau}^{(c)}(y)$, the Laplace transform of the interference is then given by

$$\mathcal{L}_{I_{ik}^{(c_0)}|\varepsilon_{ij,\tau}^{(c)}(y)}(s) \quad (16)$$

$$\begin{aligned} & = \mathbb{E} \left[\prod_{\mathbf{x} \in \Phi_{ik,\text{Tx}}^{(c_0)}} \exp \left\{ -s P_k G^{(c_0)} x^{-\alpha^{(c)}} \right\} \mid \varepsilon_{ij,\tau}^{(c)}(y) \right] \\ & \stackrel{(a)}{=} \mathbb{E}_{\Phi_{ik,\text{Tx}}^{(c_0)}} \left[\prod_{\mathbf{x} \in \Phi_{ik,\text{Tx}}^{(c_0)}} \left(\frac{1}{1 + \frac{sP_k x^{-\alpha^{(c_0)}}}{m^{(c_0)}}}} \right)^{m^{(c_0)}} \mid \varepsilon_{ij,\tau}^{(c)}(y) \right]. \end{aligned}$$

Here, (a) is obtained by averaging over the channel fading $G^{(c_0)}$, which gives the moment-generating function (MGF) of Gamma distribution. Since the density of interferer is $2\pi x \lambda_{k,\text{Tx}} \rho_{ik}^{(c_0)}(x)$, the probability generating functional (PGFL) of PPP for function $f(x)$ is obtained as [23]

$$\begin{aligned} & \mathbb{E}_{\Phi_{ik,\text{Tx}}^{(c_0)}} \left[\prod_{\mathbf{x} \in \Phi_{ik,\text{Tx}}^{(c_0)}} f(\mathbf{x}) \mid \varepsilon_{ij,\tau}^{(c)}(y) \right] \\ & = \exp \left(-2\pi\lambda_{k,\text{Tx}} \int_{\chi}^{\infty} x (1 - f(x)) \rho_{ik}^{(c_0)}(x) dx \right) \quad (17) \end{aligned}$$

where $\chi = \max(\chi_{j,k,\tau}^{(c,c_0)}, h_{ik})$ is the minimum distance bound for interferers. When the node association rule $o = r$ is used, there is no interferer with shorter distance than (8) to the receiver since a receiver selects the nearest or the strongest transmitter, and we get $\chi_{j,k,\tau}^{(c,c_0)}(y) = R_{j,k,a}^{(c,c_0)}(y)$ in (15). On the contrary, when $o = t$, a transmitter selects a receiver, so the locations of the interferers are independent with the location of the main link transmitter, and we get $\chi_{j,k,\tau}^{(c,c_0)}(y) = 0$. From (16) and (17), we get the Laplace transform of the interference as (14). ■

There is no closed form of (14). However, for the case of the interference from the transmitters in the same layer, i.e., $I_{ii}^{(c)}$, we obtain the Laplace transform of the interference in a closed form as in the following corollary.

Corollary 1: The Laplace transform of the interference from transmitters in the i -layer to the receiver in the i -layer is given by (18) when $sP_i \chi_{j,k,\tau}^{(c,c_0)}(y)^{-\alpha^{(c_0)}} < 1$ and $m^{(\text{L})} = m^{(\text{N})} = 1$, where

$$\eta = -\sqrt{\mu\nu} \ln \left(1 - \exp \left[-\frac{h_i^2}{2\xi^2} \right] \right). \quad (19)$$

Proof: From Lemma 2, the Laplace transform of the interference in the LoS environment, $I_{ii}^{(\text{L})}$, is given by

$$\begin{aligned} & \mathcal{L}_{I_{ii}^{(\text{L})}|\varepsilon_{ij,\tau}^{(c)}(y)}(s) \\ & = \exp \left\{ -2\pi\lambda_{i,\text{Tx}} \int_{\chi}^{\infty} x e^{-\eta x} \left(1 - \left(\frac{1}{1 + sP_i x^{-\alpha^{(\text{L})}}}} \right) \right) dx \right\} \\ & \stackrel{(a)}{=} \exp \left\{ 2\pi\lambda_{i,\text{Tx}} \int_{\chi}^{\infty} x e^{-\eta x} \sum_{n=1}^{\infty} (-sP_i x^{-\alpha^{(\text{L})}})^n dx \right\} \quad (20) \end{aligned}$$

$$\mathcal{L}_{I_{ii}^{(c_0)} | \varepsilon_{ij,\tau}^{(c)}(y)}(s) = \begin{cases} \exp \left[2\pi\lambda_{i,\text{Tx}} \sum_{n=1}^{\infty} (-sP_i)^n \eta^{n\alpha^{(c_0)}} - 2\Gamma \left(2 - n\alpha^{(c_0)}, \eta\chi_{j,i,\tau}^{(c,c_0)}(y) \right) \right] & (c_0) = (\text{L}) \\ \exp \left[2\pi\lambda_{i,\text{Tx}} \sum_{n=1}^{\infty} (-sP_i)^n \left\{ \frac{(\chi_{j,k,\tau}^{(c,c_0)})^{2-n\alpha^{(c_0)}}}{n\alpha^{(c_0)} - 2} - \eta^{n\alpha^{(c_0)}} - 2\Gamma \left(2 - n\alpha^{(c_0)}, \eta\chi_{j,i,\tau}^{(c,c_0)}(y) \right) \right\} \right] & (c_0) = (\text{N}) \end{cases} \quad (18)$$

$$= \exp \left\{ 2\pi\lambda_{i,\text{Tx}} \sum_{n=1}^{\infty} \left((-sP_i)^n \int_{\chi}^{\infty} x^{1-n\alpha^{(L)}} e^{-\eta x} dx \right) \right\} \\ \stackrel{(b)}{=} \exp \left\{ 2\pi\lambda_{i,\text{Tx}} \times \sum_{n=1}^{\infty} \left((-sP_i)^n \eta^{n\alpha^{(L)}} - 2 \int_{\eta\chi}^{\infty} t^{1-n\alpha^{(L)}} e^{-t} dt \right) \right\}, \quad (21)$$

where $\chi = \max(\chi_{j,i,\tau}^{(c,c_0)}(y), h_{ii}) = \chi_{j,i,\tau}^{(c,c_0)}(y)$. Here, (a) follows from the Taylor series $1/(1+x) = \sum_{n=0}^{\infty} (-x)^n$, which is convergent for $|x| < 1$, so, (20) is convergent for $sP_i x^{-\alpha^{(c)}} < 1$, and (b) follows from integration by substitution $\eta x = t$. In (21), by definition of the upper incomplete gamma function $\Gamma(x, y) = \int_y^{\infty} t^{x-1} e^{-t} dt$, we get the upper part of (18). In a similar way, the Laplace transform of the interference in the NLoS environment, $I_{ii}^{(\text{N})}$, is given by

$$\mathcal{L}_{I_{ii}^{(\text{N})} | \varepsilon_{ij,\tau}^{(c)}(y)}(s) \quad (22) \\ = \exp \left[2\pi\lambda_{i,\text{Tx}} \int_{\chi}^{\infty} x(1 - e^{-\eta x}) \sum_{n=1}^{\infty} (-sP_i x^{-\alpha^{(\text{N})}})^n dx \right] \\ = \exp \left[2\pi\lambda_{i,\text{Tx}} \sum_{n=1}^{\infty} (-sP_i)^n \left(\frac{(\chi_{j,k,\tau}^{(c,\text{N})})^{2-n\alpha^{(\text{N})}}}{n\alpha^{(\text{N})} - 2} \right) \right] \times \\ \exp \left[-2\pi\lambda_{i,\text{Tx}} \int_{\chi}^{\infty} x e^{-\eta x} \sum_{n=1}^{\infty} (-sP_i x^{-\alpha^{(\text{N})}})^n dx \right]$$

From (22), we get the lower part of (18). \blacksquare

For the i -layer receiver, the sum of total interference and noise is defined as

$$\mathcal{I}_i = \sum_{k \in \mathcal{K}, c_0 \in \{\text{L}, \text{N}\}} I_{ik,\text{Tx}}^{(c_0)} + \sigma^2 \quad (23)$$

where σ^2 is the noise power. From the property of the Laplace transform, the Laplace transform of \mathcal{I}_i is given by

$$\mathcal{L}_{\mathcal{I}_i | \varepsilon_{ij,\tau}^{(c)}(y)}(s) = \exp(-s\sigma^2) \prod_{k \in \mathcal{T}, c_0 \in \{\text{L}, \text{N}\}} \mathcal{L}_{I_{ik}^{(c_0)} | \varepsilon_{ij,\tau}^{(c)}(y)}(s). \quad (24)$$

IV. PERFORMANCE ANALYSIS OF MANS

In this section, we analyze the STP and the ASE of MAN based on the Laplace transform of the interference. In addition, we derive the upper bound of the optimal density that maximizes the STP and the ASE.

A. STP and ASE Analysis

In the event of $\varepsilon_{ij,\tau}^{(c)}(y)$, the STP is defined using signal to interference plus noise ratio (SINR) as

$$p_{ij,\tau}^{(c)}(y) = \mathbb{P} \left[\text{SINR}_{ij}^{(c)}(y) > \beta_{ij} \mid \varepsilon_{ij,\tau}^{(c)}(y) \right], \quad (25)$$

where

$$\text{SINR}_{ij}^{(c)}(y) = P_j G^{(c)} y^{-\alpha^{(c)}} / \mathcal{I}_i. \quad (26)$$

Here, β_{ij} is the target SINR, which is related to the target transmission rate between a i -layer receiver and a j -layer transmitter. In addition, the definition of ASE is given as the sum of the maximum average data rates per unit bandwidth per unit area for a specified bit error rate [32], [33]. We assume the number of the communication links in the unit area depends on the number of the transmitters and the number of the receivers for $o = t$ and $o = r$, respectively. Therefore, when $o = r$, we define the ASE as the data rate multiplied with the density of the receiver. On the contrary, when $o = t$, we define the ASE as the data rate multiplied with the density of the transmitter. Here, the data rate is $\log(1 + \beta_{ij})$ when the communication succeeds, and 0 when the communication is failed. Therefore, the STP and the ASE of the k -layer in the MAN is derived as the following Lemma.

Lemma 3: Using the node association rule τ , the STP and the ASE of the k -layer in the MAN is given as

$$\mathcal{P}_{k,\tau} = \begin{cases} \sum_{j \in \mathcal{K}, c \in \{\text{L}, \text{N}\}} f_{\mathcal{P}}(k, j, c, \tau) & \text{for } o = r, \\ \sum_{i \in \mathcal{K}, c \in \{\text{L}, \text{N}\}} f_{\mathcal{P}}(i, k, c, \tau) & \text{for } o = t, \end{cases} \quad (27) \\ \mathcal{S}_{k,\tau} = \begin{cases} \sum_{j \in \mathcal{K}, c \in \{\text{L}, \text{N}\}} (\lambda_j - \lambda_{j,o}) R_{ij} f_{\mathcal{P}}(k, j, c, \tau) & \text{for } o = r, \\ \sum_{i \in \mathcal{K}, c \in \{\text{L}, \text{N}\}} (\lambda_i - \lambda_{i,o}) R_{ij} f_{\mathcal{P}}(i, k, c, \tau) & \text{for } o = t. \end{cases} \quad (28)$$

where $R_{ij} = \log_2(1 + \beta_{ij})$ and $f_{\mathcal{P}}(i, j, c, \tau)$ is given as

$$f_{\mathcal{P}}(i, j, c, \tau) = \mathcal{A}_{ij,\tau}^{(c)} \int_{h_{ij}}^{\infty} p_{ij,\tau}^{(c)}(y) f_{Y_{ij,\tau}^{(c)}}(y) dy. \quad (29)$$

Here, $p_{ij,\tau}^{(c)}(y)$ is presented as

$$p_{ij,\tau}^{(c)}(y) = \sum_{n=0}^{m^{(c)}-1} \frac{(-s)^n}{n!} \frac{d^n}{ds^n} \mathcal{L}_{\mathcal{I}_i | \varepsilon_{ij,\tau}^{(c)}(y)}(s) \Big|_{s=l_{ij}^{(c)}(y)}, \quad (30) \\ l_{ij}^{(c)}(y) = \frac{m^{(c)} \beta_{ij}}{P_j y^{-\alpha^{(c)}}}, \quad (31)$$

where $\mathcal{L}_{\mathcal{I}_i | \varepsilon_{ij,\tau}^{(c)}(y)}(s)$ is in (24).

Proof: From (25) and (26), the STP is given by

$$p_{ij,\tau}^{(c)}(y) = \mathbb{P} \left[G^{(c)} > \frac{\beta_{ij} \mathcal{I}_i}{P_j y^{-\alpha^{(c)}}} \mid \varepsilon_{ij,\tau}^{(c)}(y) \right] \quad (32)$$

$$\stackrel{(a)}{=} \mathbb{E}_{\mathcal{I}_i} \left[\sum_{n=0}^{m^{(c)}-1} \frac{(s \mathcal{I}_i)^n}{n!} \exp(-s \mathcal{I}_i) \mid \varepsilon_{ij,\tau}^{(c)}(y) \right] \Big|_{s=l_{ij}^{(c)}(y)}$$

where (a) follows from the Gamma distribution of channel gain and the property of lower incomplete Gamma function. Notice that we derived (31) from (a). Using following property

of the Laplace transform, we obtain (30).

$$\begin{aligned}\mathcal{L}_{\mathcal{I}_i}(s) &= \mathbb{E}_{\mathcal{I}_i} [\exp(-s\mathcal{I}_i)], \\ (-\mathcal{I}_i)^n \mathcal{L}_{\mathcal{I}_i}(s) &= \frac{d^n}{ds^n} \mathcal{L}_{\mathcal{I}_i}(s).\end{aligned}\quad (33)$$

Therefore, from the PDF of the main link distance and the association probability in Lemma 1, we obtain the STP of node in the k -layer as (27). Furthermore, by the definition of the ASE, which is the data rate multiplied with the density of the node in the k -layer, we obtain ASE of k -layer AN in the MAN as (28). ■

In the MAN, the STP and the ASE of the network is given by

$$\mathcal{P}_{\text{MAN},\tau} = \begin{cases} \sum_{i \in \mathcal{K}} \frac{\lambda_{i,\text{Rx}}}{\lambda_{T,\text{Rx}}} \mathcal{P}_{i,\tau} & \text{for } o = \text{r}, \\ \sum_{i \in \mathcal{K}} \frac{\lambda_{i,\text{Tx}}}{\lambda_{T,\text{Tx}}} \mathcal{P}_{i,\tau} & \text{for } o = \text{t}, \end{cases} \quad (34)$$

$$\mathcal{S}_{\text{MAN},\tau} = \sum_{i \in \mathcal{K}} \mathcal{S}_{i,\tau}. \quad (35)$$

Note that the STP of the MAN is defined as the average STP of the receivers(transmitters), whereas the ASE of the MAN is defined as the total amount of data rate per unit frequency per area.

The STP and the ASE have multiple integral which makes evaluation hard, however, the integral in the Laplace transform can be removed under the condition, which explained in the following remark.

Remark 1: In Lemma 3, the Laplace transform of the interference from the same layer of AN can be replaced with (18) when $\tau = \text{rs}$, $\beta_{ij} < 1$, $m^{(L)} = m^{(N)} = 1$, and $B_k = P_k$, since the conditions in Corollary 1 are satisfied.

Proof: In the event of $\varepsilon_{ij,\tau}^{(c)}(y)$, using the node association $\tau = \text{rs}$, $\chi_{j,k,\tau}^{(c,c_0)}(y) = R_{j,k,a}^{(c,c_0)}$. Furthermore, when $B_k = P_k$, $\frac{P_k x^{-\alpha(c_0)}}{P_j y^{-\alpha(c)}} < 1$ for all $R_{j,k,a}^{(c,c_0)} \leq x$. Therefore, $l_{ij}^{(c)}(y) P_k x^{(c_0)} = \beta_{ij} \frac{P_k x^{-\alpha(c_0)}}{P_j y^{-\alpha(c)}} < 1$, which satisfy the condition in Corollary 1. ■

B. Upper Bound of Optimal Density

In the design of the MAN, it is important to optimize the densities of transmitters in order to maximize the STP and the ASE.³ However, it is hard to present the STP or the ASE in a closed form, so, consequently, hard to obtain the optimal densities. Nevertheless, we derived the upper bound of the optimal density that maximizes the STP and the ASE in the following corollary.

Corollary 2: When j -layer transmitters communicate to k -layer receivers and the channel coefficient is $m^{(N)} = m^{(L)} = 1$, the upper bound of the optimal transmitter density in the j -layer that maximizes the STP, $\lambda_{j,\text{Tx}}^{b,\mathcal{P}_{k,\tau}}$, and that maximizes the ASE, $\lambda_{j,\text{Tx}}^{b,\mathcal{S}_{k,\tau}}$, of the k -layer are respectively given by

$$\lambda_{j,\text{Tx}}^{b,\mathcal{P}_{k,\tau}} = \begin{cases} \frac{1}{2\pi\epsilon_{kj}} & \text{for } o = \text{r}, \\ 0 & \text{for } o = \text{t}, \end{cases} \quad (36)$$

³Note that the optimal density of the receiver is trivial to derive. From our analysis, $\mathcal{P}_{k,\text{ra}}$ is independent with the density of the receiver. Furthermore, $\mathcal{P}_{k,\text{ta}}$ and $\mathcal{S}_{k,\tau}$ increase with the density of the receiver.

TABLE II
SIMULATION PARAMETERS

Parameter	Value	Parameter	Value
$(m^{(L)}, m^{(N)})$	(1, 1)	(μ, ν, ξ)	$(0.5, 3 \times 10^{-4}, 20)$
$(\alpha^{(L)}, \alpha^{(N)})$	(2.5, 3.5)	(a, b)	(12.0910, 0.1139)
a	$a = s$	β_k	0.7
(B_k, P_k)	1	Receiver layer	0
σ^2	0	Transmitter layer	j, k

$$\lambda_{j,\text{Tx}}^{b,\mathcal{S}_{k,\tau}} = \begin{cases} \frac{1}{2\pi\epsilon_{kj}} & \text{for } o = \text{r}, \\ 0 & \text{for } o = \text{t and } k \neq j, \\ \max_{i \in \mathcal{K}} \left[\frac{1}{2\pi\epsilon_{ki}} \right] & \text{for } o = \text{t and } k = j. \end{cases} \quad (37)$$

where ϵ_{ij} is

$$\epsilon_{ij} = \int_{h_{ij}}^{\infty} x \left(1 - \frac{\rho_{ij}^{(L)}(x)}{1 + \beta_{ij} h_{ij}^{\alpha^{(L)}} x^{-\alpha^{(L)}}} - \frac{\rho_{ij}^{(N)}(x)}{1 + \beta_{ij} h_{ij}^{\alpha^{(N)}} x^{-\alpha^{(N)}}} \right) dx. \quad (38)$$

Proof: See Appendix A. ■

Note that the optimal density exists due to the trade-off: increasing the transmitter density increases the ASE or STP due to the shorter link distance and the increasing number of communication links in the network, while also decreases the ASE or STP due to the larger interference. However, when $o = \text{t}$, the STP always decreases with the transmitter density since the main link distance distribution is determined by the receiver density not by the transmitter density, which gives the optimal transmitter density as zero. Furthermore, when $o = \text{t}$ and $j \neq k$, the ASE of j -layer always decreases with the k -layer transmitter density since neither the main link distance nor the number of communication links in the j -layer depend on the k -layer transmitter density.

As the optimal density of the transmitters is hard to be presented, we need to use a certain search algorithm such as the exhaustive search. In that case, this upper bound can be usefully used to determine the search range. In addition, as shown in Corollary 2, the optimal transmitter density bound can be determined for each layer independently as it is not affected by other layer transmitter densities. From Corollary 2, we can also see the following tendency of the upper bound.

Corollary 3: The upper bound of the optimal transmitter densities $\lambda_{j,\text{Tx}}^{b,\mathcal{P}_{k,\tau}}$ and $\lambda_{j,\text{Tx}}^{b,\mathcal{S}_{k,\tau}}$, are non-increasing function of h_{ij} under the conditions of $\beta_{ij} h_{ij}^{\alpha^{(L)}} > 1$ and $h_{ij} > 1$, since ϵ_{ij} increases with h_{ij} .

Proof: See Appendix B. ■

Note that the condition $\beta_{ij} h_{ij}^{\alpha^{(L)}} > 1$ and $h_{ij} > 1$ are conditions, which are generally satisfied in UAV communications. From Corollary 3, we can see that as the altitude difference between the transmitter and the receiver h_{ij} increases, the optimal transmitter density bound becomes smaller, which will be almost zero for large altitude difference.

V. NUMERICAL RESULTS

In this section, we present the STP and the ASE of the MAN for the receiver-oriented and the transmitter-oriented

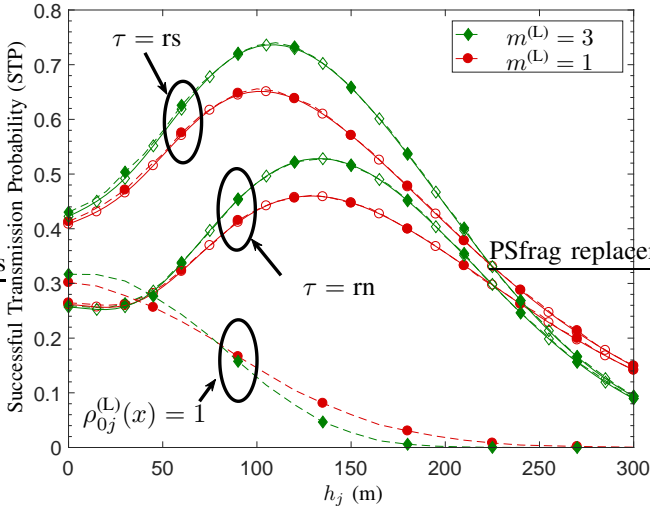


Fig. 3. STP of the single layer AN according to the transmitter altitude h_j with different LoS coefficients $m^{(L)}$ when $\lambda_j = 10^{-5}$, $o = r$.

association cases. For the numerical results, we consider the interference-limited environment, i.e., $\sigma^2 = 0$, in order to clarify the results. We use the ground layer, i.e., 0-layer, and i -layer as receivers' layer, j -layer and k -layer as the transmitters' layers, and omit the subscripts Rx and Tx for the simplicity, e.g., $\lambda_0 = \lambda_{0,Rx}$ and $\lambda_j = \lambda_{j,Tx}$. Furthermore, we omit the subscript in the total transmitter density, i.e., $\lambda_j + \lambda_k = \lambda_T$ instead of $\lambda_{T,Tx}$. Simulation parameters for our numerical results summarized in Table. II, where Fig. 3 uses $m^{(L)} = 3$ and the nearest distance association, i.e., $a = n$, and Fig. 4 uses the i -layer as the receivers' layer.

A. Receiver-oriented Association Case

In this subsection, we show the STP of the MAN when the receiver-oriented association is considered. We omit the ASE results since the ASE is a multiplication of the STP with the receiver density when $o = r$, which gives the same tendency with the STP. To show the effects of network parameters on the performance more clearly, we first show the performance for a single layer AN case in Figs. 3-5, and then provide the performance for a two layer MAN case in Fig. 6.

Figure 3 shows the STP of the single layer AN (i.e., the j -layer) as a function of the altitude of the layer h_j for different values of channel coefficient $m^{(L)} = \{1, 3\}$ and two node association rules, i.e., the strongest power ($\tau = rs$) and the nearest distance ($\tau = rn$) associations. Here, the density of the transmitter is $\lambda_j = 10^{-5}$ [nodes/m²]. The LoS probability in (2) is used for this figure, and we also provide the results with $\rho_{0j}^{(L)} = 1$ (i.e., the case that always assumes LoS link) to show the effect of the LoS probability consideration. Simulation results are obtained from Monte Carlo simulation which are presented by the dashed lines with filled markers, while analysis results are presented by the solid lines with unfilled markers, which fit well with the simulation results.

From Fig. 3, we observe the existence of the optimal altitude of the transmitter layer due to the trade-off by the

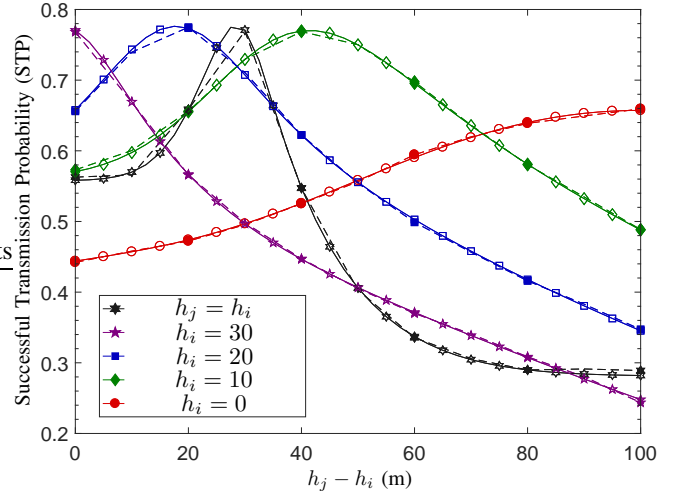


Fig. 4. STP of the single layer AN according to the difference of altitude between layers $h_j - h_i$ with different receiver altitudes h_i when $\lambda_j = 10^{-5}$ and $\tau = rs$.

altitude on the STP: as the altitude of the transmitter increases, the LoS probability of the main link also increases, which results in higher STP, while both the LoS probability of the interference link and the main link distance increase, which lowers STP. However, when the LoS probability is $\rho_{0j}^{(L)} = 1$ and not changed with the altitude, the STP only decreases since the main link distance increases with the altitude.

In addition, we observe the effect of the LoS coefficient $m^{(L)}$ on the STP, which gives higher STP at low altitude region (e.g., $h_j < 200$) and gives lower STP at high altitude region (e.g., $h_j > 230$). For the Nakagami- m fading, the larger coefficient $m^{(c)}$ gives less chance to have the smaller channel gain. At the low altitude region, the main link is mostly LoS while the interference is NLoS that gives the higher SINR with the larger LoS coefficient $m^{(L)}$. On the contrary, at the high altitude region, the interference has more LoS links that gives the lower SINR with the larger LoS coefficient $m^{(L)}$.

Figure 4 depicts the STP of the single-layer AN⁴ as a function of the altitude difference between the j -layer (i.e., transmitter layer) and the i -layer (i.e., receiver layer), $h_j - h_i$, for different altitudes of the i -layer, $h_i = \{0, 10, 20, 30\}$, when $h_j > h_i$. Here, the strongest power association ($\tau = rs$) is used and $\lambda_j = 10^{-5}$. The simulation results are presented by the dashed lines with filled markers, while analysis results are presented by the solid lines with unfilled markers. For the analysis results, we use Lemma 2 for $h_i = \{0, 10, 20, 30\}$ and Corollary 1 for the case of $h_i = h_j$, and show that analysis results match well with the simulation results.⁵

From Fig. 4, we observe that the optimal altitude difference $(h_j - h_i)^*$ that maximizes the STP exists and decreases with the h_i . When h_i is large, the LoS probability of the main link and the interfering links are high, hence, the smaller distance

⁴Even though we use two ANs, i and j -layer, we regard it as the single-layer AN since only one layer acts as the transmitter and the receiver.

⁵Although the closed form Laplace transform contains the infinite summation in Lemma 2 and we use partial summation, i.e., $\sum_{n=1}^{10}$, instead of $\sum_{n=1}^{\infty}$, we show high coincidence with simulation results since the partial summation converges to the infinite sum with a bearable error.

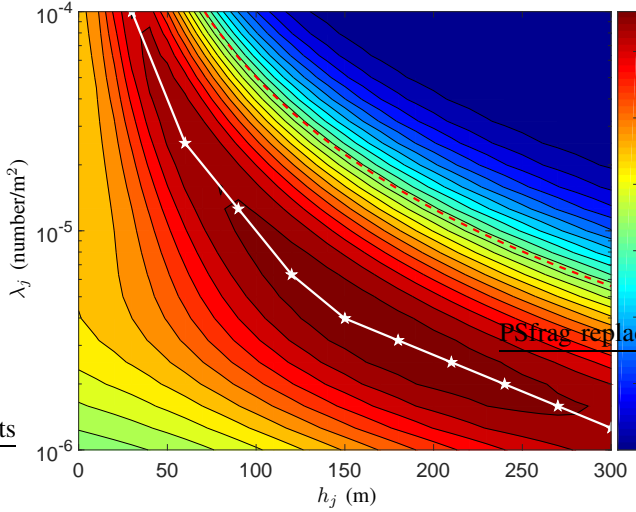


Fig. 5. STP of the single layer AN as functions of the transmitter density λ_j and the transmitter altitude h_j when $\tau = rs$. A solid line with stars presents the optimal density and a dotted line presents the upper bound of the optimal density.

gives the higher STP that reduce optimal $h_j - h_i$. Therefore, the difference between altitudes should be smaller when the communication between different ANs in high altitude is considered. Considering $h_i = h_j$, which is the same with the communication between nodes in the same layer, optimal altitude of layer h_i exist since the LoS probability of the main link and the interfering links increases with h_i . At low altitude region (e.g., $h_i = 0$), the channel is mostly NLoS, at high altitude region (e.g., $h_i = 100$), contrary, the channel is mostly LoS. In between low and high (e.g., $h_i = 30$), the LoS probability is high when the smaller horizontal distance is considered, therefore, the main link is under LoS channel whereas the interfering links are under NLoS channel, that gives the higher STP compared with the low and high altitude.

Figure 5 shows the STP of the single-layer AN as functions of the transmitter density λ_j and the transmitter altitude h_j when $\tau = rs$. We present the optimal density λ_j^* that maximizes the STP using a solid line with stars and the upper bound of the optimal density, obtained from Corollary 2, as a dashed line. In addition, we observe the existence of the optimal density since as the density of the transmitter increases, the main link distance decreases and the LoS probability of the main link increases, which results in higher STP, while both the interfering nodes and the LoS probability of the interferers increase, which results in lower STP.

Furthermore, by comparing the optimal density and the upper bound of the optimal density, we notice that their trends according to the altitude h_j are similar. Specifically, both the optimal density and its upper bound decrease with the altitude h_j as proven in Corollary 3. Although the difference between the optimal density and its upper bound is not small, the upper bound can play an important to find the optimal density by restricting the searching range, e.g., exhaustive searching starting from the upper bound.

Figure 6 shows the STP of the two layer MAN as functions of the density of j -layer transmitters λ_j and the density of k -

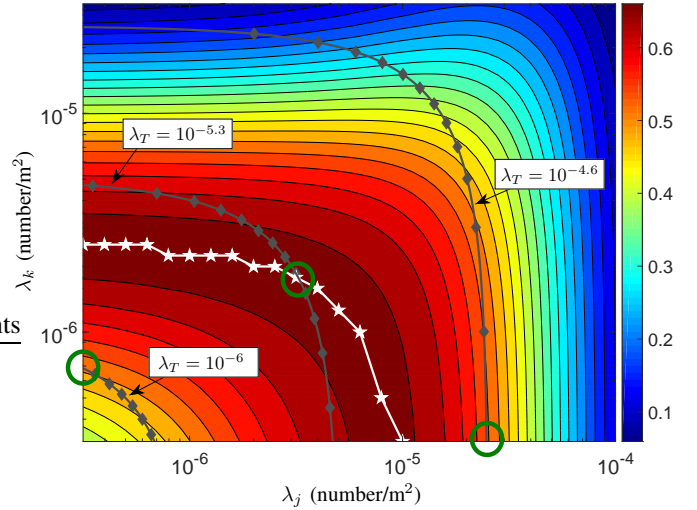


Fig. 6. STP of the two layer MAN as functions of the j -layer transmitter density λ_j and the k -layer transmitter density λ_k when $h_j = 100$, $h_k = 200$, and $\tau = rs$. A line with stars presents the optimal j -layer transmitter density and a line with diamonds presents the area that have the same total density λ_T .

layer transmitters λ_k , when $h_j = 100$, $h_k = 200$, and $\tau = rs$. The line marked with stars shows the optimal transmitter density of the k -layer λ_k^* for different values of λ_j . We can see that λ_k^* decreases as λ_j increases. This is because the larger interference from the j -layer that makes the density of other interfering layer to decrease (i.e., k -layer), for the optimal density. The lines marked with diamonds show the cases of having the given values of the total density, i.e., $\lambda_j + \lambda_k = \lambda_T$, and the points of circles shows the optimal densities $(\lambda_j, \lambda_k)^*$ for each cases of λ_T . We can see that when λ_T is large (e.g., $\lambda_T = 10^{-4.6}$), having all transmitters in the layer with lower altitude (i.e., the j -layer) can achieve higher STP, while for small λ_T (e.g., $\lambda_T = 10^{-6}$), having all transmitters in the layer with higher altitude (i.e., the k -layer) achieves higher STP. However, when λ_T is neither large or small, e.g., $\lambda_T = 10^{-5.3}$, having transmitters in multiple layers, i.e., both j and k -layers can be better in terms of the STP.

B. Transmitter-oriented Association Case

In this subsection, we show the STP and the ASE of the MAN when the transmitter-oriented association and the ground receiver in the 0-layer with density $\lambda_0 = 10^{-5}$ is considered. We show the performance for a single layer AN case in Figs. 7 and 8, and then provide the performance for a two layer MAN case in Figs. 9 and 10.

Figures 7 and 8 show the STP and ASE of the single layer AN as functions of the transmitter density λ_j and their altitude h_j when $\tau = rs$. The solid line with squares presents the optimal altitudes h_j^* that maximize STPs (in Fig. 7) and the solid line with stars presents the optimal density λ_j^* that maximizes ASE (in Fig. 8) for different values of λ_j . The dashed line in Fig. 8 presents the upper bound of the optimal transmitter density, obtained from Corollary 2. Note that the same as the receiver-oriented association case, the optimal transmitter density and its upper bound have the same trend,

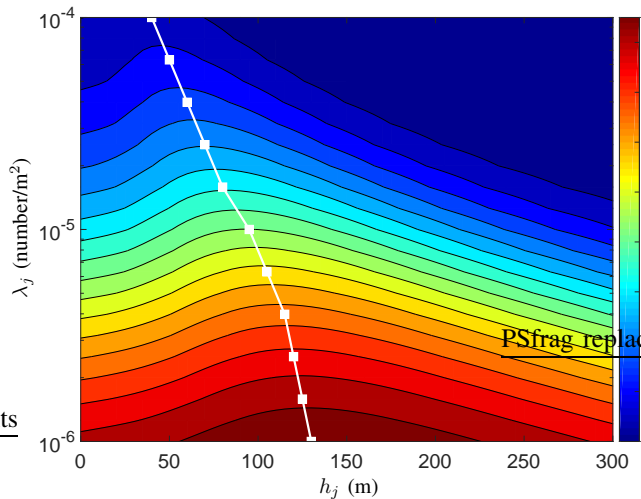


Fig. 7. STP of the single layer AN as functions of the transmitter density λ_j and the transmitter altitude h_j when $\tau = \text{ts}$. A solid line with squares presents the optimal altitude.

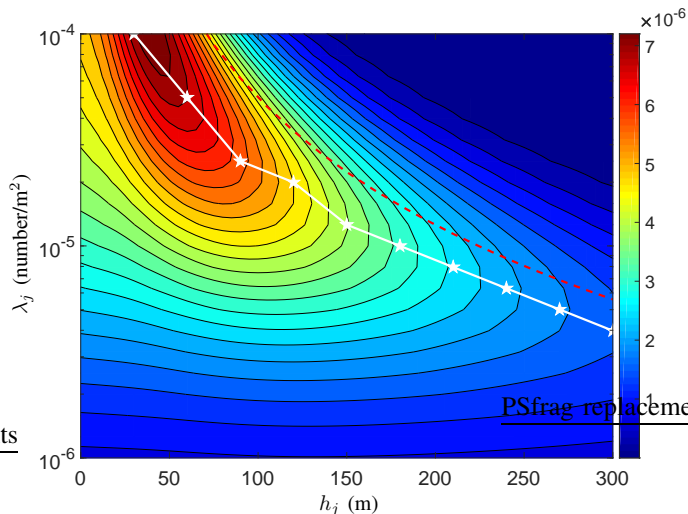


Fig. 8. ASE of the single layer AN as functions of the transmitter density λ_j and the transmitter altitude h_j when $\tau = \text{ts}$. A solid line with stars presents the optimal density and a dotted line presents the upper bound of the optimal density.

which decreases with the altitude of the AN. Furthermore, in Fig. 8, we can see that the optimal transmitter density in terms of the ASE exists due to following reasons. For small transmitter density λ_j , when λ_j increases, the impact of increasing number of the transmitting links in the network is large, so ASE increases with λ_j . However, for large λ_j , when λ_j increases, the impact of increasing interfering nodes and increasing their LoS probabilities to a receiver becomes more critical than the increasing number of the transmitting links, so the ASE decreases with λ_j . Note that the optimal transmitter density in terms of the STP is zero, since the larger transmitter density gives the more interfering nodes, while the main link distance is not changed (as the transmitter-oriented association is used).

Figure 9 shows the ASE of the two layer MAN as functions of the j -layer transmitter density λ_j and the k -layer transmitter density λ_k when $h_j = 100$, $h_k = 200$, and $\tau = \text{ts}$. The line

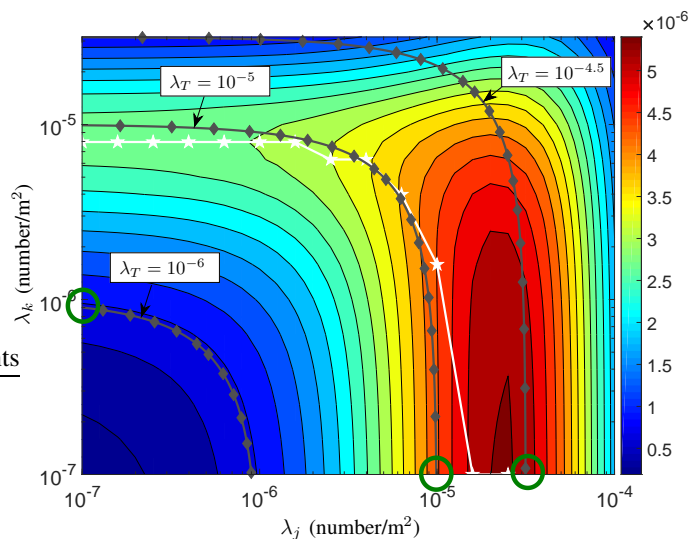


Fig. 9. ASE of the two layer MAN as functions of the j -layer transmitter density λ_j and the k -layer transmitter density λ_k when $h_j = 100$, $h_k = 200$, and $\tau = \text{ts}$. A line with stars presents the optimal j -layer transmitter density and a line with diamonds presents the area that have the same total density λ_T .

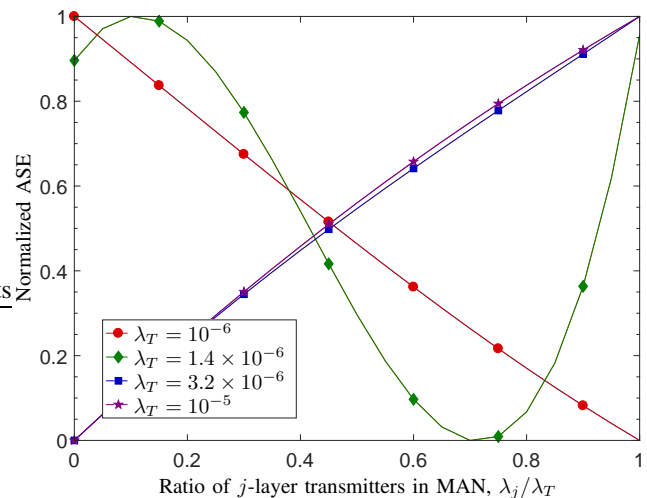


Fig. 10. Normalized ASE of two layer MAN according to the ratio of the j -layer transmitter density to the total density λ_j/λ_T with different total densities. λ_T when $h_j = 100$, $h_k = 200$, and $\tau = \text{ts}$.

marked with stars shows the optimal transmitter density of the k -layer λ_k^* for different values of λ_j . The lines marked with diamonds show the cases of having given values of the total transmitter density, i.e., $\lambda_j + \lambda_k = \lambda_T$, and the optimal density pairs, i.e., $(\lambda_j, \lambda_k)^*$ is marked with circles for different λ_T . From Fig. 9, we can see that when λ_T is large (e.g., $\lambda_T = 10^{-5}$ and $\lambda_T = 10^{-4.5}$), $\lambda_j^* > 0$ and $\lambda_k^* = 0$. However, when λ_T is small (e.g., $\lambda_T = 10^{-6}$), $\lambda_k^* > 0$ and $\lambda_j^* = 0$.

In order to further clarify the relationship between the total transmitter density λ_T and the optimal densities of each layers, we present the normalized ASE in Fig. 10 as a function of the ratio of the j -layer transmitter density to the total density λ_j/λ_T for different values of the total density λ_T . Here the

normalized ASE, $\mathcal{S}_{\lambda_T}^{\mathcal{N}}(\rho)$, is defined as

$$\mathcal{S}_{\lambda_T}^{\mathcal{N}}(\rho) = \frac{\mathcal{S}_{\lambda_T}(\rho) - \min_{\rho'} \mathcal{S}_{\lambda_T}(\rho')}{\max_{\rho'} \mathcal{S}_{\lambda_T}(\rho') - \min_{\rho'} \mathcal{S}_{\lambda_T}(\rho')} \quad (39)$$

where $\mathcal{S}_{\lambda_T}(\rho)$ is the ASE when the total density λ_T and the ratio of j -layer transmitter density, $\rho = \lambda_j/\lambda_T$, is given. Here, the normalized ASE is a linear transform that makes the ASE to have values between $[0, 1]$, for the optimal ratio visualization. From Fig. 10, we can see that when the total transmitter density λ_T is high, the optimal is to use the lower AN only, i.e., $\lambda_j^* = \lambda_T$. On the other hand, when λ_T is low, the optimal is to use the higher AN only, i.e., $\lambda_k^* = \lambda_T$. However, when λ_T is neither high nor low such as $\lambda_T = 1.4 \times 10^{-6}$, it is better to use the two layer MAN instead of the single layer AN, which is the same as the STP of the MAN with the receiver-oriented association.

VI. CONCLUSION

This paper establishes a foundation for the MAN accounting for the different UAV densities, altitudes, and transmission power in each layer AN. After modeling the MAN with the association rules and the channel, suitable for various scenario of the MAN, we newly analyze the association probability, the main link distance distribution, and the Laplace transform of the interference. We then analyze the STP and the ASE of the MAN, and also provide the upper bounds of the optimal UAV densities that maximize the STP and the ASE, which is decreasing with the altitude of the AN and determined independently without the effect of other layer UAV densities. Finally, in the numerical results, we provide insights on the efficient design of the MAN. Specifically, we show that the optimal altitude of each AN, maximizing the ASE, decreases with the UAV density, and also the optimal UAV density decreases with the altitude of the AN. The optimal UAV density of each AN, maximizing the STP, also decreases with the altitude of the AN for the receiver-oriented association case, while it becomes zero for the transmitter-oriented association case. We also show that when the total density of the UAVs is given, the optimal design of the MAN is single AN with the lower and the higher altitudes for large and small total densities, respectively, whereas the optimal design is to use the multiple layers when the density is neither large nor small.

APPENDIX

A. Proof of Corollary 2

In order to derive the upper bound of the optimal densities, we get the derivatives of the STP and the ASE with respect to the transmitter density. Then, we obtain the range of the densities that reduce the STP and the ASE, which gives the upper bound. In this proof, we use following notation, which is not used in the rest of the paper.

$$\mathcal{C}_{ij,\tau}^{(c)}(y) = \mathcal{A}_{ij,\tau}^{(c)} p_{ij,\tau}^{(c)}(y) f_{Y_{ij,\tau}^{(c)}}(y) \quad (40)$$

1) *receiver-oriented Association*: From Lemma 3, when $o = r$, the derivative of the k -layer STP with respect to the j -layer transmitter density is given by

$$\frac{\partial}{\partial \lambda_{j,\text{Tx}}} \mathcal{P}_{k,\tau} = \sum_{i \in \mathcal{K}, c \in \{\text{L}, \text{N}\}} \int_{h_{ki}}^{\infty} \frac{\partial \mathcal{C}_{ki,\tau}^{(c)}(y)}{\partial \lambda_{j,\text{Tx}}} dy, \quad (41)$$

$$\frac{\partial \mathcal{C}_{ki,\tau}^{(c)}(y)}{\partial \lambda_{j,\text{Tx}}} = \begin{cases} \frac{\mathcal{C}_{ki,\tau}^{(c)}(y)}{\lambda_{j,\text{Tx}}} \left(1 - \lambda_{j,\text{Tx}} \phi_{kj,\tau}^{(c)}(i, y)\right) & \text{for } i = j, \\ -\frac{\mathcal{C}_{ki,\tau}^{(c)}(y)}{\lambda_{j,\text{Tx}}} \phi_{kj,\tau}^{(c)}(i, y) & \text{for } i \neq j, \end{cases} \quad (42)$$

$$\phi_{kj,\tau}^{(c)}(i, y) = \quad (43)$$

$$2\pi \sum_{c_0 \in \{\text{L}, \text{N}\}} \left[\int_{h_{ki}}^{\infty} x \rho_{ki}^{(c_0)}(x) dx - \int_{\chi}^{\infty} \frac{x \rho_{ki}^{(c_0)}(x)}{1 + l_{ki}^{(c)}(y) P_i x^{-\alpha^{(c_0)}}} dx \right]$$

where, $\chi = \max(\chi_{j,i,\tau}^{(c,c_0)}(x), h_{ki})$. When $i \neq j$, (42) is always negative. Furthermore, when $i = j$, if the following inequality holds, (42) is the negative.

$$\max_{y,c} \left[\frac{1}{\phi_{kj,\tau}^{(c)}(j, y)} \right] \leq \lambda_{j,\text{Tx}} \quad (44)$$

Here, $\phi_{kj,\tau}^{(c)}(j, y)$ increases with y and $\phi_{kj,\tau}^{(\text{L})}(j, y) < \phi_{kj,\tau}^{(\text{N})}(j, y)$, therefore, $\phi_{kj,\tau}^{(c)}(j, y)$ has minimum at the $c = (\text{L})$ and $y = h_{kj}$, of which minimum is given by

$$\epsilon_{kj} = \phi_{kj,\tau}^{(\text{L})}(j, h_{kj}). \quad (45)$$

Therefore, when $1/\epsilon_{kj} \leq \lambda_{j,\text{Tx}}$, the STP of the k -layer is always decreased with the density of the transmitter in the j -layer, which gives the upper bound of the optimal density that maximizes the STP. In addition, the derivative of the ASE is given by

$$\frac{\partial}{\partial \lambda_{j,\text{Tx}}} \mathcal{S}_{k,\tau} = \lambda_{k,\text{Rx}} \sum_{i \in \mathcal{K}, c \in \{\text{L}, \text{N}\}} \int_{h_{ki}}^{\infty} R_{ki} \frac{\partial \mathcal{C}_{ki,\tau}^{(c)}(y)}{\partial \lambda_{j,\text{Tx}}}. \quad (46)$$

The density of the receiver and the data rate are independent with the density of the transmitter. Therefore, if the inequality (44) holds, the ASE decreases with the density of the transmitter, which gives the same upper bound of the density that maximizes the STP.

2) *transmitter-oriented Association*: When $o = t$, the derivative of the STP of the k -layer with respect to the density of the j -layer transmitter is given by

$$\frac{\partial}{\partial \lambda_{j,\text{Tx}}} \mathcal{P}_{k,\tau} = \sum_{i \in \mathcal{K}, c \in \{\text{L}, \text{N}\}} \int_{h_{ik}}^{\infty} \frac{\partial \mathcal{C}_{ik,\tau}^{(c)}(y)}{\partial \lambda_{j,\text{Tx}}} \quad (47)$$

$$\frac{\partial \mathcal{C}_{ik,\tau}^{(c)}(y)}{\partial \lambda_{j,\text{Tx}}} = -\mathcal{C}_{ik,\tau}^{(c)}(y) \theta_{kj,\tau}^{(c)}(i, y) \quad (48)$$

$$\theta_{kj,\tau}^{(c)}(i, y) = \quad (49)$$

$$2\pi \sum_{c_0 \in \{\text{L}, \text{N}\}} \int_{\chi}^{\infty} x \rho_{ij}^{(c_0)}(x) \left(1 - \frac{1}{1 + l_{ij}^{(c)}(y) P_j x^{-\alpha^{(c_0)}}}\right) dx,$$

where $\chi = \max(\chi_{k,j,\tau}^{(c,c_0)}, h_{ij})$. Therefore, the STP always decreases with the transmitter density, which gives the optimal density as zero. In addition, the derivative of the ASE is given

by

$$\frac{d}{d\lambda_{j,\text{Tx}}} \mathcal{S}_{k,\tau} = \sum_{i \in \mathcal{K}, c \in \{\text{L}, \text{N}\}} \int_{h_{ik}}^{\infty} R_{ki} \frac{\partial}{\partial \lambda_{j,\text{Tx}}} \left(\lambda_{k,\text{Tx}} \mathcal{C}_{ik,\tau}^{(c)}(y) \right), \quad (50)$$

$$\frac{\partial \left(\lambda_{k,\text{Tx}} \mathcal{C}_{ik,\tau}^{(c)}(y) \right)}{\partial \lambda_{j,\text{Tx}}} = \begin{cases} \mathcal{C}_{ik,\tau}^{(c)}(y) \left(1 - \lambda_{j,\text{Tx}} \theta_{kj,\tau}^{(c)}(i, y) \right) & \text{for } k = j, \\ -\lambda_{k,\text{Tx}} \mathcal{C}_{ik,\tau}^{(c)}(y) \theta_{kj,\tau}^{(c)}(i, y) & \text{for } k \neq j. \end{cases} \quad (51)$$

When $k \neq j$, the gradient is always negative which gives the optimal density as 0. When $k = j$, the range of the density that gives negative gradient is given by

$$\max_{i,y,c} \left[\frac{1}{\theta_{kj,\tau}^{(c)}(i, y)} \right] \leq \lambda_{j,\text{Tx}}. \quad (52)$$

Note that we maximize over $i \in \mathcal{K}$. Here, as $\theta_{kj,\tau}^{(c)}(i, y)$ increases with y and $\theta_{kj,\tau}^{(\text{N})}(i, y) < \theta_{kj,\tau}^{(\text{L})}(i, y)$, the minimum is given as

$$\epsilon_{ki} = \theta_{kj,\tau}^{(\text{L})}(i, h_{ki}). \quad (53)$$

Therefore, we get the upper bound of the transmitter density that maximize the STP and the ASE.

B. Proof of Corollary 3

From Corollary 2, ϵ_{ij} is given by

$$\epsilon_{ij} = \int_0^{\infty} y (1 - q(y, h_{ij})) dy, \quad (54)$$

$$q(y, h_{ij}) = \frac{\varrho_{ij}^{(\text{L})}(y)}{1 + \frac{\beta_{ij} h_{ij}^{\alpha(\text{L})}}{(y^2 + h_{ij}^2)^{\alpha(\text{L})/2}}} + \frac{\varrho_{ij}^{(\text{N})}(y)}{1 + \frac{\beta_{ij} h_{ij}^{\alpha(\text{N})}}{(y^2 + h_{ij}^2)^{\alpha(\text{N})/2}}}.$$

We use the integration by substitution for ϵ_{ij} as $y^2 = x^2 - h_{ij}^2$, hence, the modified LoS probability is $\varrho_{ij}^{(\text{L})}(y) = \rho_{ij}^{(\text{L})} \left(\sqrt{y^2 + h_{ij}^2} \right)$ which increase with h_{ij} for given y . Therefore, ϵ_{ij} increases with h_{ij} if $q(y, h_{ij})$ decreases with h_{ij} for all $y \in [0, \infty)$. The function $q(y, h_{ij})$ is further reformulated as

$$q(y, h_{ij}) = \left(1 + \beta_{ij} \left(\frac{h_{ij}^2}{h_{ij}^2 + y^2} \right)^{\alpha(\text{L})/2} \right)^{-1} + \frac{\varrho_{ij}^{(\text{N})}(y) \beta_{ij} h_{ij}^{\alpha(\text{L})} \left((h_{ij}^2 + y^2)^{\alpha(\text{N})/2} - (h_{ij}^2 + y^2)^{\alpha(\text{L})/2} \right)}{\left(\beta_{ij} h_{ij}^{\alpha(\text{L})} + (h_{ij}^2 + y^2)^{\alpha(\text{N})/2} \right) \left(\beta_{ij} h_{ij}^{\alpha(\text{L})} + (h_{ij}^2 + y^2)^{\alpha(\text{L})/2} \right)} \quad (55)$$

We use $\varrho_{ij}^{(\text{L})}(y) + \varrho_{ij}^{(\text{N})}(y) = 1$. The upper part decreases with h_{ij} since $\frac{h_{ij}^2}{h_{ij}^2 + y^2}$ increases with h_{ij} . Furthermore, the lower part decreases with h_{ij} if $1 < h_{ij}^2 + y^2$ and $1 < \beta_{ij} h_{ij}^{\alpha(\text{L})}$. Therefore, ϵ_{ij} decreases with h_{ij} if $1 < h_{ij}$ and $1 < \beta_{ij} h_{ij}^{\alpha(\text{L})}$.

REFERENCES

[1] D. Kim, J. Lee, and T. Q. S. Quek, "Performance analysis for multi-layer unmanned aerial vehicle networks," in *Proc. IEEE Global Telecomm. Conf.*, Abu Dhabi, UAE, Dec. 2018, pp. 1–6.

[2] Y. Zeng, R. Zhang, and T. J. Lim, "Wireless communications with unmanned aerial vehicles: opportunities and challenges," *IEEE Commun. Mag.*, vol. 54, no. 5, pp. 36–42, May 2016.

[3] N. H. Motlagh, M. Bagaa, and T. Taleb, "UAV-based IoT platform: A crowd surveillance use case," *IEEE Commun. Mag.*, vol. 55, no. 2, pp. 128–134, May 2017.

[4] Y. Zeng, R. Zhang, and T. J. Lim, "Throughput maximization for UAV-enabled mobile relaying systems," *IEEE Transactions on Communications*, vol. 64, no. 12, pp. 4983–4996, Sep. 2016.

[5] A. Al-Hourani, S. Kandeepan, and S. Lardner, "Optimal lap altitude for maximum coverage," *IEEE Wireless Commun. Lett.*, vol. 3, no. 6, pp. 569–572, Jul. 2014.

[6] A. Al-Hourani, S. Kandeepan, and A. Jamalipour, "Modeling air-to-ground path loss for low altitude platforms in urban environments," in *Proc. IEEE Global Telecomm. Conf.*, Austin, TX, Feb. 2014, pp. 2898–2904.

[7] Z. Yang, L. Zhou, G. Zhao, and S. Zhou, "Blockage modeling for inter-layer UAVs communications in urban environments," in *Proc. Int. Conf. Telecommun.*, 2018, pp. 307–311.

[8] M. Mozaffari, W. Saad, M. Bennis, and M. Debbah, "Unmanned aerial vehicle with underlaid device-to-device communications: Performance and tradeoffs," *IEEE Trans. Wireless Commun.*, vol. 15, no. 6, pp. 3949–3963, Feb. 2016.

[9] C. Liu, T. Q. S. Quek, and J. Lee, "Secure UAV communication in the presence of active eavesdropper," in *Proc. IEEE International Conference on Wireless Communications and Signal Processing. Conf.*, Nanjing, China, 2017, pp. 1–6.

[10] M. Kim and J. Lee, "Impact of an interfering node on unmanned aerial vehicle communications," *arXiv preprint arXiv:1903.08154*, Mar. 2019. [Online]. Available: <https://arxiv.org/pdf/1903.08154.pdf>

[11] M. M. Azari, Y. Murillo, O. Amin, F. Rosas, M.-S. Alouini, and S. Pollin, "Coverage maximization for a poisson field of drone cells," in *Proc. IEEE Int. Symp. on Personal, Indoor and Mobile Radio Commun.*, Feb. 2017, pp. 1–6.

[12] M. Alzenad and H. Yanikomeroglu, "Coverage and rate analysis for unmanned aerial vehicle base stations with LoS/NLoS propagation," in *Proc. IEEE Global Telecomm. Conf.*, Abu Dhabi, UAE, Dec. 2018, pp. 1–7.

[13] T. Hou, Y. Liu, Z. Song, X. Sun, and Y. Chen, "Multiple antenna aided NOMA in UAV networks: A stochastic geometry approach," *IEEE Transactions on Communications*, vol. 67, no. 2, pp. 1031–1044, Oct. 2019.

[14] J. Li and Y. Han, "Optimal resource allocation for packet delay minimization in multi-layer UAV networks," *IEEE Communications Letters*, vol. 21, no. 3, pp. 580–583, Nov. 2017.

[15] S. Sekander, H. Tabassum, and E. Hossain, "Multi-tier drone architecture for 5G/B5G cellular networks: Challenges, trends, and prospects," *IEEE Commun. Mag.*, vol. 56, no. 3, pp. 96–103, Mar. 2018.

[16] C. Zhang and W. Zhang, "Spectrum sharing in drone small cells," in *Proc. IEEE Global Telecomm. Conf.*, Washington, DC, Feb. 2016, pp. 1–6.

[17] L. Qi, S. Yan, and M. Peng, "Modeling and performance analysis in UAV assisted ultra dense networks," in *Proc. IEEE International Conference on Communications. Conf.*, Jul. 2018, pp. 1–6.

[18] H. Wu, X. Tao, N. Zhang, and X. Shen, "Cooperative UAV cluster-assisted terrestrial cellular networks for ubiquitous coverage," *IEEE J. Sel. Areas Commun.*, vol. 36, no. 9, pp. 2045–2058, Aug. 2018.

[19] M. M. Azari, F. Rosas, A. Chiumento, and S. Pollin, "Coexistence of terrestrial and aerial users in cellular networks," in *Proc. IEEE Global Telecomm. Conf.*, Dec. 2017, pp. 1–6.

[20] R. Arshad, L. Lampe, H. ElSawy, M. Hossain *et al.*, "Integrating UAVs into existing wireless networks: A stochastic geometry approach," in *Proc. IEEE Global Telecomm. Conf.*, Dec. 2018, pp. 1–6.

[21] A. M. Hayajneh, S. A. R. Zaidi, D. C. McLernon, M. Di Renzo, and M. Ghogho, "Performance analysis of UAV enabled disaster recovery networks: A stochastic geometric framework based on cluster processes," *IEEE Access*, vol. 6, pp. 26215–26230, May 2018.

[22] E. Turgut and M. C. Gursoy, "Downlink analysis in unmanned aerial vehicle (UAV) assisted cellular networks with clustered users," *IEEE Access*, vol. 6, pp. 36313–36324, May 2018.

[23] M. Haenggi, R. K. Ganti *et al.*, "Interference in large wireless networks," *Foundations and Trends in Networking*, vol. 3, no. 2, pp. 127–248, 2009.

[24] S. Chandrasekharan, K. Gomez, A. Al-Hourani, S. Kandeepan, T. Rasheed, L. Goratti, L. Reynaud, D. Grace, I. Bucaille, T. Wirth *et al.*, "Designing and implementing future aerial communication networks," *IEEE Commun. Mag.*, vol. 54, no. 5, pp. 26–34, May 2016.

- [25] H. S. Dhillon, R. K. Ganti, F. Baccelli, and J. G. Andrews, "Modeling and analysis of K-tier downlink heterogeneous cellular networks," *IEEE J. Sel. Areas Commun.*, vol. 30, no. 3, pp. 550–560, Apr. 2012.
- [26] S. Singh, H. S. Dhillon, and J. G. Andrews, "Offloading in heterogeneous networks: Modeling, analysis, and design insights," *IEEE Trans. Wireless Commun.*, vol. 12, no. 5, pp. 2484–2497, Apr. 2013.
- [27] Q. Zhang, H. H. Yang, T. Q. S. Quek, and J. Lee, "Heterogeneous cellular networks with LoS and NLoS transmissions: the role of massive MIMO and small cells," *IEEE Trans. Wireless Commun.*, vol. 16, no. 12, pp. 7996–8010, Sep. 2017.
- [28] B. Galkin, J. Kibilda, and L. A. DaSilva, "A stochastic geometry model of backhaul and user coverage in urban UAV networks," *arXiv preprint arXiv:1710.03701*, Oct. 2017. [Online]. Available: <https://arxiv.org/pdf/1710.03701.pdf>
- [29] P. Series, "Propagation data and prediction methods required for the design of earth-space telecommunication systems," *Recommendation ITU-R*, pp. 618–12, 2015.
- [30] T. Bai, R. Vaze, and R. W. Heath, "Analysis of blockage effects on urban cellular networks," *IEEE Transactions on Wireless Communications*, vol. 13, no. 9, pp. 5070–5083, Jun. 2014.
- [31] H. Cho, C. Liu, J. Lee, T. Noh, and T. Q. S. Quek, "Impact of elevated base stations on the ultra-dense networks," *IEEE Commun. Lett.*, pp. 1268–1271, Apr. 2018.
- [32] M.-S. Alouini and A. Goldsmith, "A unified approach for calculating error rates of linearly modulated signals over generalized fading channels," *IEEE Trans. Commun.*, vol. 47, no. 9, pp. 1324–1334, Sep. 1999.
- [33] V. Chandrasekhar and J. G. Andrews, "Spectrum allocation in tiered cellular networks," *IEEE Trans. Commun.*, vol. 57, no. 10, pp. 3059–3068, Oct. 2009.